Chemistry and Materials Research
ISSN 2224- 3224 (Print) ISSN 2225- 0956 (Online)
Vol.10 No.2, 2018
www.iiste.org

Alternating Current Electrophoretic Deposition of Hydroxyapatite Composite Coating on Mg-0.8wt.%Ca-3%wt.%Zn alloy

Yahia Sarhan[4] Maamoun Abel Hamid[1] Yasser K. Abdel-Monem[2] Fakiha Heakal[3] I.M.Ghayad[1*]
1.Central Metallurgical Research & Development Institute
2.Fac. of Science, Menofia University
3.Fac. of Science, Cairo University
4.Alnasr Co for Intermediate Chemicals

Abstract
The present work investigates the AC electrophoretic deposition of nano-sized HAP composite coating on Mg-0.8wt.%Ca-3%wt.%Zn alloy. Nano HAP powder was prepared using hydrothermal microwave assisted technique. HAP coating is deposited electrophoretically from dispersing medium (ETELAC) forming composite coating on the alloy surface. Electrophoretic deposition experiments were conducted as single run (S), double run (D) and multirun (M). The properties of HAP coating regarding adhesion, morphology and corrosion behavior were thoroughly investigated.Results show that the best coating regarding the weight gain as well as the morphology was obtained from multi run (M) experiments of 5%HAP and 5% ETELAC at 200 V under 150 rpm stirring. Electrochemical Impedance (EIS) investigation show that HAP composite coating posses a high corrosion resistance compared to the substrate alloy. The mechanism of HAP/ETELAC coating formation was thoroughly discussed.

1. Introduction

Implants were manufactured from stainless steel [1], titanium alloys [2], polymers [3] have the drawback of exposing the patient to a second operation to remove the implant specially in joining of bone fracture healing. Moreover, the difference in hardness between the human bone and the implant might result in osteoporosis. In addition, the alloy also may be incapable of forming a chemical bond with bone directly. As it implanted the immune system will surround it by fibrous capsule just a way to isolate it from the body.

Recently, some polymers and magnesium alloys are considered to be an excellent biodegradable implants. Since, polymers are expensive and lack the required mechanical strength, magnesium alloys offers a promising alternative to the above materials. Magnesium alloys possess a density of 1.74-1.84 g/cm^3 which is close to that of the natural bone1.8-2.1 g/cm^3 and their compressive strengths are much higher than those of biodegradable polymers. It is biologically compatible and enhances cell growth and bone formation. The major drawback of Mg is its high corrodibility in the presence of chloride ions producing magnesium ions and hydrogen gas shifting the pH of a solution to higher values. Coating is the main path to overcome these drawbacks [4-6].

Hydroxiapatite (HAP) having the formula $Ca_{10}(PO_4)_6(OH)_2$, amounts to 65 % of the total bone mass, with the remaining mass formed by organic matter "mostly collagen" and water. HAP is a biological active material which has extensive biomedical applications. Hydroxyapatite has been developed as a coating on metallic implants in the field of orthopedics and dentistry due to its chemical and biological similarity to human hard tissues as well as direct bonding capability to the surrounding tissues [4], [5]. It has been established that HAP coating can promote more rapid fixation and stronger bonding between the host bone and the implant.

HAP coating provides protection to the implant substrate against corrosion in the biological environment, and acts as barrier against the release of metal ions from the substrate into the environment. What is more inspiring is that HAP coating can enhance bone growth across a gap of 1 mm between the bone and the implant and it is capable of limiting the formation of any fibrous membrane and converting a motion-induced fibrous membrane in to a bony anchorage [6].

Numerous applications of AC-EPD have two major characteristics [7]: (i) AC-EPD to suppress water hydrolysis at high voltages in inorganic (ceramic) coatings and (ii) AC-EPD for deposition of biological entities where AC-EPD showed a more uniform and denser microstructure

The present work investigates the AC electrophoretic deposition of nano-sized HAP composite coating on Mg-0.8wt.%Ca-3%wt.%Zn alloy. HAP coating is deposited electrophoretically from dispersing medium forming composite coating on the alloy surface. The effect of HF pretreatment as well as the influence of coating parameters, such as pH, agitation, deposition voltage, temperature and conductivity were studied. The properties of HAP coating regarding adhesion, morphology and corrosion behavior were thoroughly investigated.

2. Experimental

Mg-0.8wt.%Ca-3%wt.%Zn alloy was used as the substrate material. The alloy was prepared from pure Mg (99.99%), Zinc (99.98%) and Ca (99.98%) using a laboratory resistance furnace. Zn and Ca were selected as alloying elements because they are essential elements to human. Disc specimens whose diameter is 24 mm were prepared from the alloy and further cut into 4 quarter cylindrical shapes with 10 cm^2 area for each quarter. Specimens were polished using SiC papers up to 1200 grit and then washed by distilled water and finally dried in hot air.

2.1. Preparation of nano HAP powder using hydrothermal microwave assisted

Nano HAP powder was prepared using pure chemicals shown in Table (1). 0.1 M EDTA as Disodium salt solution was prepared in distilled water. Since calcium carbonate ($CaCO_3$) is sparingly soluble in water, equi molar ratio of $CaCO_3$ (0.1 mole) was added stepwise to the EDTA solution with continuous stirring to achieve a final concentration of 0.1 M Ca-EDTA as stable complex. While keeping stirring a 0.06 M of anhydrous Disodium phosphate (Na_2HPO_4) solution was added drop wise and finally 0.1 M solution of Sodium Hydroxide (NaOH) was added to the overall solution to reach a final pH of 12.8-13. The overall solution was transferred to the microwave (800 Watt-2.45 GHz) for 20 minutes. The solution was taken from the microwave after the formation of the precipitate and left for cooling, then filtered using 42 whatmann filter paper. The ppt was washed with hot bidistilled water to remove any sodium hydroxide molecules. Then the ppt was dried in the dryer to obtain a fine powder. The prepared nano Hap was characterized using XRD technique (BRUKER-Germany).

Table (1): Chemicals used in HAP synthesis

Materials	Chemical formula	Functions	Suppliers
Calcium Carbonate	($CaCO_3$)	Calcium ion source	(Flucka, Garantie)
Di-Sodium Hydrogen Phosphate Anhydrous	(Na_2HPO_4)	Phosphate ion source	ADWIC
Ethylene Diamine Tetra Acetic Acid as Disodium salt	(EDTA)	Calcium complexing and masking agent	ACROS Organic
Sodium Hydroxide	(NaOH)	Adjusting pH value	ADWIC

2.2. Electrophoretic Deposition

The prepared nano HAP was dispersed in a solution of ETELAC (HAWKING Electrotechnology Limited,UK) as resin solution which contains 1-Methoxy-2-Propanol and Ethylene Glycol Monohexyl Ether as dispersants. Suspensions of concentrations of 5% ETELAC + 5% HAP, 2.5% ETELAC+ 5 % HAP, and 2.5 % ETELAC + 2.5 % HAP were used for electrophoretic deposition experiments. Physical properties regarding agglomeration and zeta potential measurements were performed. In the agglomeration test, a solution of 2 wt.% of HAP in water in the absence and in the presence of 2 wt.% ETELAC was vigorously stirred for different times and 50 ml was taken by means of graduated cylinder and left for agglomeration and the time taken for precipitation was recorded.

A schematic diagram for the electrophoresis deposition cell is shown in Fig. 1. It consists of two electrodes system including hollow circular AISI 316 L stainless steel used as the counter electrode against Mg alloy. The cell was connected to a SMART POWER (PLKCN) variator used as AC power supply for AC-EPD. The two electrodes are placed in a glass beaker of 1000 ml capacity. Magnetic stirrer was used for adjusting velocity of stirring the dispersing media. A thermometer used for measuring the temperature of the deposition medium.

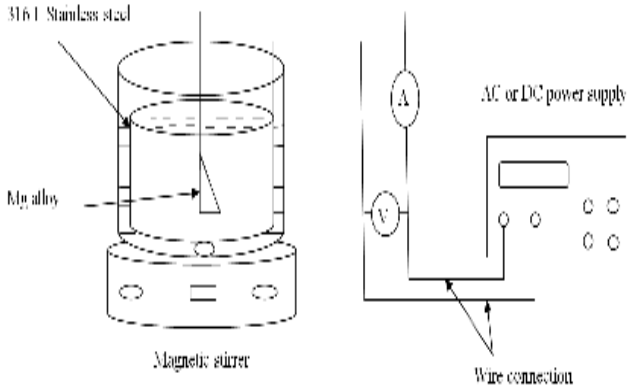

Fig. 1. Schematic representation of cell construction used for EPD

Prior to HAP coating, Mg specimens were ultrasonicated in acetone for 1 min., rinsed in distilled water and

then immersed in Hydrofluoric acid HF (40%) followed by rinsing in distilled water and drying in hot air. Specimens were electrophoretically coated using alternating current (AC) with single, double, and multi runs while current density was recorded by current/volt multimeter. Upon reaching the steady value of current density the experiment at definite AC-voltage was stopped. Agitation of the solution took place using mechanical stirrer at 150 r.p.m.

All coated samples were immersed in water to remove any impurities, dried in air and finally cured in a dryer at 130 ^{0}C for 30 min then cooled in open atmosphere. Temperature above 130 ^{o}C may cause further decomposition for ETELAC according to its usage instructions. The phase structure of HAP coatings specimens were investigated using XRD technique whereas the surface morphology and chemical composition of the coating were investigated using the Field Emission Scanning Electron Microscope (FESEM) equipped with Energy Dispersive X-Ray (EDX) unit.

The adhesion of the HAP coating was tested using adhesion tape testing method which is a quick identifier that assesses the adhesion between the coating layer and magnesium alloys substrate by applying and removing pressure-sensitive tape over "X" cuts made using Elcometer Cross Hatch Cutter in the coating film. The test carried out according to ASTM D3359 standard test methods for measuring adhesion by Tape Test. The test was performed as follows:

- An X-cut is made through the film with a carbide tip tool to the substrate.
- Pressure-sensitive tape is applied over the cut.
- Tape is smoothed into place by using a pencil eraser over the area of the incisions.
- Tape is removed by pulling it off rapidly back over itself as close to an 180º.

The test results were classified to six grades outlined below:

5A: no removal or peeling.
4A: Trace peeling or removal along incisions.
3A: Jagged removal along incisions up to 1.6 mm on either side.
2A: Jagged removal along incisions up to 3.2 mm on either side.
1A: Removal from most of the area of the X under the tape.
0A: Removal beyond the area of the X.

Electrochemical impedance spectroscopy (EIS) tests were performed on the coated specimens. All tests were carried out using Autolab potentiostat/Galvanostat (PGSTAT30) specified for electrochemical measurements. A conventional three-electrode cell, (a single compartment-glass cell of 250 ml capacity was used with platinum as counter electrode). The working electrodes were the coated specimens with an exposed area of 0.196 cm^2. All samples were measured with respect to saturated calomel electrodes (SCE). The electrolyte solution is simulated body fluid (SBF) whose chemical composition is shown in Table (2). Measurements were performed at pH = 7.4 and 37 ^{0}C [8]. EIS experiments were performed over a frequency range from 0.1Hz to 65 kHz with an amplitude of 0.01 V with respect to the corrosion potential (E_{corr}). Prior to testing the specimen was immersed for 15 min. in the SBF solution to acquire a steady potential (E_{corr}).

Table (2): Chemical composition of simulated body fluid (SBF)

Chemicals	NaCl	KCl	$CaCl_2$	$NaHCO_3$	$MgSO_4.7H_2O$	KH_2PO_4	Na_2HPO_4	Glucose
Wt.(gm/l)	8.8	0.4	0.14	0.35	0.2	0.1	0.06	1

3. Results and Discussions

3.1. HAP powder characterization

HAP is characterized by the Ca/P ratio to be 1.67 [8-9], so it is desirable to maintain this ratio during preparation process to achieve a stoichiometric structure of the formed HAP. Direct combination of calcium source with phosphate source leads to the formation of tricalcium phosphate. EDTA as Disodium salt affects the masking of calcium cation from direct reaction with phosphate anion [10-11]. The process can be represented by the following equations:

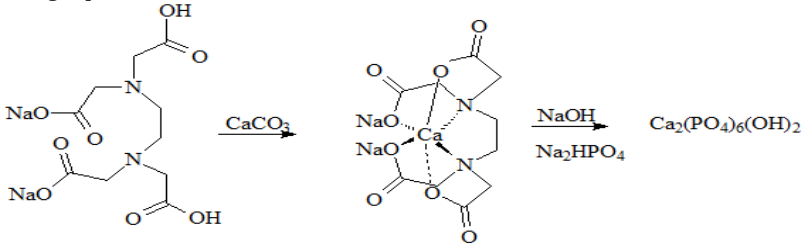

(1)

$$0.1\ M\ Na_2EDTA + 0.1\ M\ CaCO_3 \longrightarrow 0.1\ M\ Na_2EDTA\text{-}Ca + H_2O + CO_2 \quad (2)$$

$$Na_2EDTA\text{-}Ca + 0.06\ M\ Na_2HPO_4 + 0.1\ M\ NaOH \longrightarrow Ca_{10}(PO_4)_6(OH)_{2\ ppt} \quad (3)$$

EDTA as disodium salt is hexa dentate ligand, possesses six functional groups, four carboxyl groups and

two amino groups, reacting with divalent cations with equimolar ratio. EDTA is good chelating agent for calcium ions which forming a stable complex. EDTA is able to form simultaneously several coordination bonds with metal ions forming polychelate complexes. The doubly charged metal ions replace two hydrogen atoms of the carboxyl groups in Na_2EDTA and simultaneously coordinately bonded to the nitrogen atoms of the amino groups, thus forming very stable five-membered rings. Hence, preventing both calcium ions and phosphate ions from direct reaction with each other utilizing the masking of calcium ions by EDTA and prevent the direct formation of tricalcium phosphate. Using calcium carbonate helps to avoid the formation of byproduct during the preparation of HAP. EDTA reacts with an equimolar ratio of $CaCO_3$ and calcium ions replace the protons of carboxylic groups forming a stable complex and carbonic acid as a byproduct. Carbonic acid dissociates rapidly giving water molecules with the evolution of carbon dioxide gas. The addition of Na_2HPO_4 as phosphate ion source together with the addition of NaOH as source of hydroxide ions that is necessary for the complete formation of calcium hydroxy apatite [12-13]. Finally, utilizing the energy of microwave radiation accelerates the rate of HAP formation through direct interaction of microwave as electromagnetic radiation and the polar solvent leading to aligning the dipoles of the water polar molecules. This enables water molecules to absorb radiation, rotate and gain very high energy enough for the formation of HAP [14].

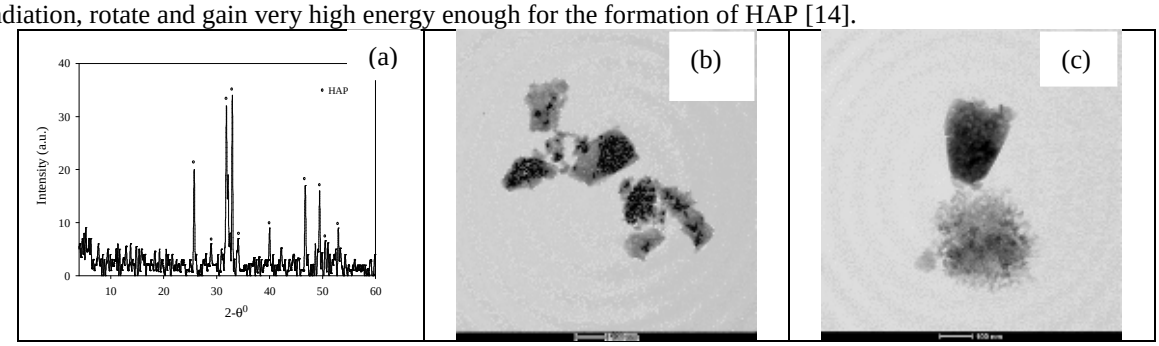

Fig. 2. (a) XRD pattern of prepared HAP, (b) and (c) TEM graph of nano HAP

The peak at 2-θ^0 angle equals 31.813^0 corresponds to a d-value equals 2.8106 A^0 which is characteristic to HAP that corresponding to (211) plane with intensity equals 33.6. All previous results revised according to reference code (JCPDS card 01-076-0694) that corresponds to characteristic chart of calcium hydroxy apatite. TEM graph exhibits flakes like structure in nano scale.

3.2. Agglomeration test results

The results of agglomeration test are presented in Table (3). It is shown that the addition of 2 wt.% ETELAC enhance the HAP suspension stability in solution. The presence of ETELAC increases the residence time of HAP more than two times.

Table (3): Results of agglomeration test

Agglomerate/ cm^3	0.5 cm^3	1cm^3	2 cm^3
In absence of TELAC			
Time of agglomeration	55 sec	110 sec	220 sec
In presence of TELAC			
Time of agglomeration	120 sec	180 sec	480 sec

3.3. Zeta potential measurements

Results of zeta potential measurements are shown in Table (4). It is obvious that the values of zeta potential of HAP in water do not give sufficient value for electrophoretic deposition as the value do not exceed -17.5 mV. Zeta potential increases by introducing ETELAC up to +59.3 mV at pH = 7. This value is more favorable for EPD where the particles give more appreciable response to the applied voltage. ETELAC changes the overall charge on the plane of shear of HAP particles in water from its originally negative to positive allowing cathodic deposition of HAP on Mg alloy substrate. The reversal of plane of shear charge is probably due to the electrostatic adsorption of oppositely charged ETELAC constituents on the particle surfaces. Moreover, alcoholic constituents may donate the proton which leads to increasing the double layer thickness and increasing zeta potential [15-16]. Finally, the the most favored pH is about 7.

Table (4): Zeta potential measurements

HAP in water				
pH	5	7	9	11
Zeta pot.(mV)	-11.4	-11.3	-11.8	-17.5
HAP in water containing ETELAC				
pH	5	6	7	8
Zeta pot.(mV)	43.6	52.3	59.3	56.4

3.4. Results of ACEPD experiments

After **AC-EPD** coating, samples were visually evaluated and according to the weight gain derived from the equation:

$$w_g = \frac{w_c - w_o}{A} \quad (4)$$

Where w_g is the weight gain, w_c the weight of coated sample, w_o the weight of uncoated samples, and A is the surface area.

AC-EPD coating is beneficial due to the fact that; the absence of bubble formation as water decomposition is minimized and the nucleation of bubbles is prevented under AC fields [17].

5%ETELAC + 5%HAP solution was selected to carry out EPD experiments because its zeta potential value is excellent. Samples were coated electrophoretically at different AC-voltages. At each potential, the sample was subjected to the coating process until the current reaches a steady value or diminishes to zero indicating no more coating formation. Then the sample was removed from the bath and dried. This run is defined as Single Run (S). Single Run experiments serve to determine the minimum current consumed during the formation of insulating layer. Above this current, the formed coating film can be degraded due to the vigorous evolution of hydrogen gas which can remove or decrease the adhesion of coating film to the base metal. The time for each single run is inversely proportional to the applied potential. At each potential, 3 samples were coated; the first represents Single Run and termed in this work as S; the second was additionally coated for 2 minute and this is Double Run experiment and termed as (D); the third sample is coated for 2 min (multi-run) and is termed M. During multi-run, the sample was emerged from the suspension every 20 second, dried and immersed into the solution again.

3.4.1. Effect of applied voltage

The applied voltage varied from 10 V to 200 V using 5% ETELAC + 5% HAP suspension. The results of weight gains at each applied voltage are recorded in Figure 3.

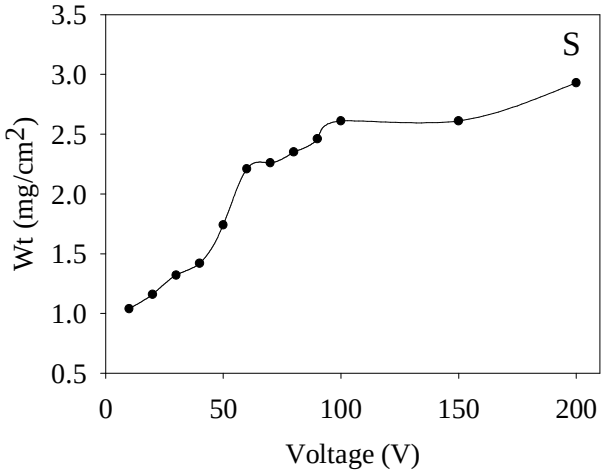

Fig. 3: Weight gain at different applied voltages using 5%ETELAC + 5%HAP suspension obtained from single run experiments with stirring at 150 rpm

As seen from Figure 3; weight gain increases increases with the increase of applied potential. At higher voltages, the deposition thickness grows more rapidly and consequently the voltage drop from formation of barrier layer takes place in a shorter time [18-19]. Formed ETELAC/HAP composite coatings don't give homogeneous morphology instead they give large porous sponge structure at applied voltage starts from 70 V.

Weight gain is calculated at each applied voltage for double and multi run deposition experiments using 5%ETELAC+5%HAP suspension and the results are recorded in Figure 4. Figure 4 reveals the increase of weight gain with the increase of applied voltage for D experiments up to 90 V where further increase in applied voltage inversely affects the coating process. Multi run experiments gives more homogeneous morphology of

ETELAC/HAP composite coatings and their corresponding weight gains are the highest amongst all experiments at all applied voltage. 200 V gives the best weight gain because of the presence of sufficient driving forces that enable the HAP particle reaching the electrodes. It can be stated that increasing the time increases the weight gain [20].

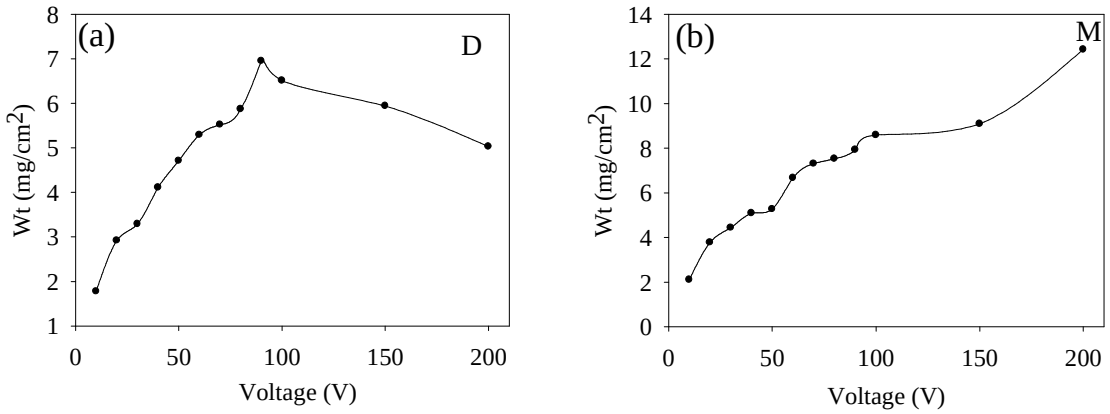

Fig. 4: Weight gain against applied voltage for (a) D and (b) M experiments using 5% ETELAC + 5% HAP suspension

Multi Run experiments introduced to overcome the defects observed in S and D experiments. Continuous drying of the coating gives more homogeneity of the produced coating formed from ETELAC/HAP composite coating and probably resulting in the formation of multilayer coating. This is noted from the continuous decrease of the consumed current density during each coating process (Table 5).

Table (5): Current densities variation at time intervals at each applied voltage

Time / Voltage	0 : 20 (sec)	20 : 40 (sec)	40 : 60 (sec)	60 : 80 (sec)	80 : 100 (sec)	100 : 120 (sec)
10 V	2.4 : 1.8	1.8 : 1.2	1.2 : 0.8	0.8 : 0.6	0.6 : 0.5	0.5 : 0.2
20 V	8.0 : 7.0	6.8 : 6.0	6.0 : 5.2	5.1 : 4.2	4.2 : 2.9	2.9 : 0.8
30 V	16.0 : 14.2	13.9 : 11.8	11.6 : 10	9.7 : 7.8	6.8 : 4.1	4.1 : 1.8
40 V	22 : 20	19.8 : 14.1	13.6 : 10.6	9.6 : 7.2	6.8 : 4.0	4.0 : 2.0
50 V	25 : 21.2	21 : 18.4	18.1 : 15.7	15.5 : 10.2	10 : 6.7	6.5 : 2.4
60 V	32.4 : 26.8	25.4 : 23.4	22.1 : 18.2	16.4 : 12.4	9.6 : 6.7	5.7 : 3.1
70 V	38.4 : 30	30 : 23	23 : 17.6	16.9 : 11.1	10.6 : 7.1	6.8 : 3.5
80 V	46 : 36	36 : 27	26 : 21	21 : 14	14 : 8.2	8.1 : 4.3
90 V	55 : 48	48 : 39	38 : 29	28 : 16	15 : 8	8.0 : 5.5
100 V	62 : 52	52 : 44	44 : 36	35 : 25	25 : 14	14 : 6.2
150 V	69 : 58	58 : 59	49 : 40	40 : 31	31 : 24	24 : 7.0
200 V	78 : 61	61 : 47	46 : 32	31 : 20	19 : 17	11 : 8

The recorded data show the decrease of current densities at all applied voltages indicating formation of ETELAC/HAP composite coating. The drying of the sample before each run gives good coverage of the coating on the substrate. At high voltages, high current densities were obtained. This can be attributed to the high EMF created at high voltages which drags the particles to the electrode surface more rapidly resulting in more coating formation.

Experiments were also carried out using 2.5%ETELAC + 5%HAP and 2.5%ETELAC + 2.5%HAP suspensions to show the effect of concentration of HAP and ETELAC. Experiments are carried out as multi run since as it gives the best results. Results are recorded in Figure 5.

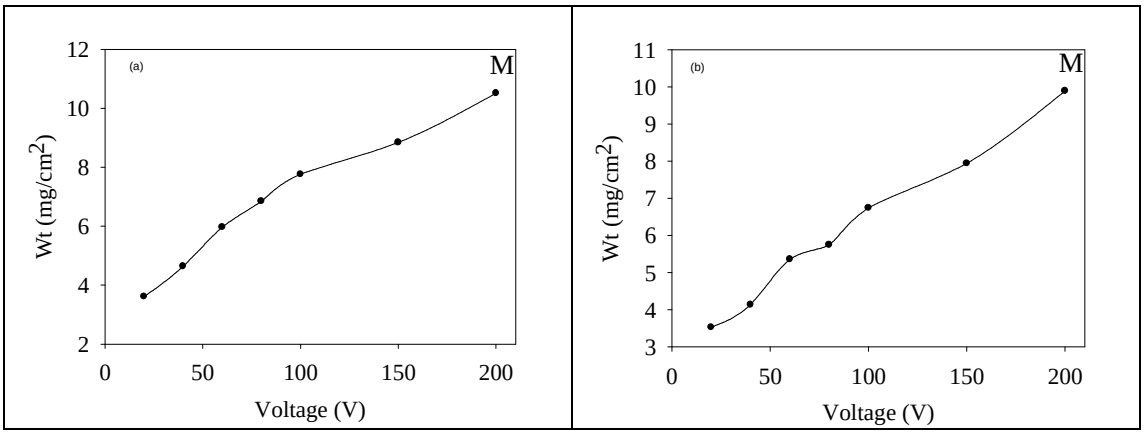

Fig. 5. Weight gain at all applied voltages for M experiments with stirring at 150 r.p.m using (a)2.5%ETELAC + 5%HAP and (b) 2.5%ETELAC + 2.5%HAP suspensions

Comparing these results with that obtained from 5%ETELAC + 5%HAP suspension; it is obvious that weight gain decreased and the morphology of coating are not god as that observed using 5%ETELAC + 5%HAP suspension (Figure 6). High concentration enables particles to reach the electrode more rapidly decreasing the diffusion layer which enhance the particles to reach isoelectric point near the electrode, i.e., zero zeta potential and the suspension reaches its maximum instability, i.e., particle coagulate on the substrate leading to the growth of the deposit. Inversely, the diffusion layer becomes thicker and the particles reach their IEP at a longer distance from the substrate and therefore low deposition occurs in case of 2.5 % ETELAC + 5 % HAP and 2.5 % ETELAC + 2.5 % HAP suspension [21-24].

The weight gain decreases according to the following order:

5%ETELAC + 5%HAP > 2.5%ETELAC + 5%HAP > 2.5%ETELAC + 2.5%HAP

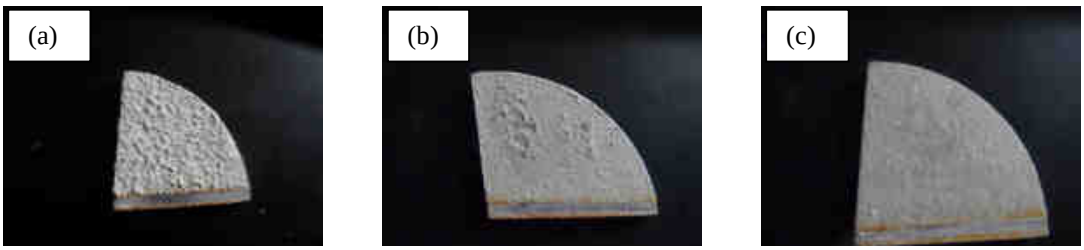

Fig. 6. Images of coated samples of M experiments using (a) 5 % ETELAC + 5 % HAP suspension, (b) 2.5 % ETELAC + 5 % HAP suspension and (c) 2.5 % ETELAC + 2.5 % HAP suspension with stirring at 150 r.p.m

3.4.2. Surface characterization of ETELAC/HAP composite coating

3.4.2.1. XRD characterization of ETELAC/HAP composite coating

The corresponding peaks of Mg-0.8%Ca-3%Zn alloy (Fig. 7) illustrate the presence of peaks due to Mg, and $Ca_2Mg_6Zn_3$ phase which formed on grain boundary [25]. High intensity of the peaks due to high crystallinity of Mg.

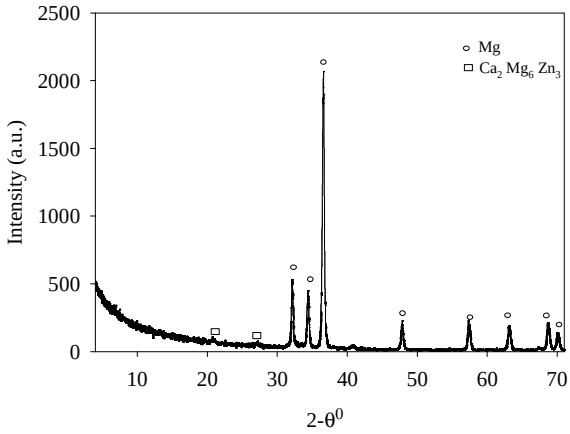

Fig. 7: XRD chart of base Mg-0.8%Ca-3%Zn alloy

XRD of coated samples (Figure 8) reveals that peaks due to base Mg disappeared or weakened where HAP peaks are prevailed. HAP characteristic peaks appear at 2θ equals 31.813 which correspond to a d-value equals 2.8106 A^o. The intensity of the peaks is higher for coated samples using 5%ETELAC+5%HAP suspension (550 counts/sec) compared to that coated using 2.5%ETELAC+5%HAP suspension (450 counts/sec). This indicates the efficiency of coating process and good surface coverage of the magnesium alloy by ETELAC/HAP composite coating. The high intensity of HAP peaks at 5%ETELAC + 5%HAP may be attributed to more crystalline HAP deposition or more dense ETELAC/HAP composite coating. Increased intensity of the HAP coated magnesium alloy more than that of HAP powder (see Fig. 2) may be due to the increase in the crystallinity after curing the Mg coated samples. The representative peaks are only for HAP and there are no any other representative peaks for polymer matrix due to its non-crystalline nature.

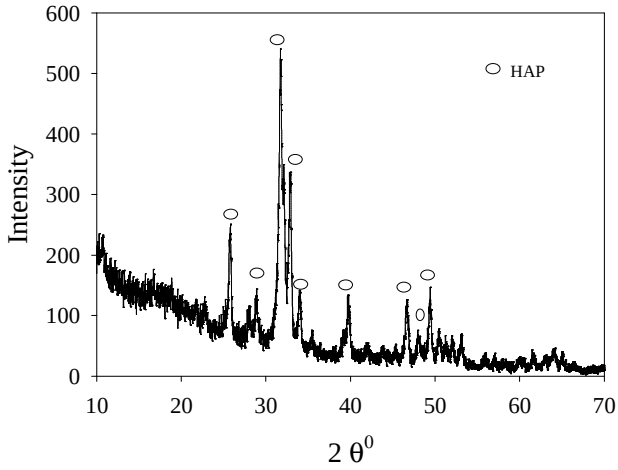

Figure 8: XRD of HAP coatings obtained using (a) 2.5% ETELAC+5%HAP
(b) 5%ETELAC+5%HAP suspensions with stirring at 150 r.p.m

3.4.2.2. SEM and EDX characterization

EDX spectra of base Mg alloy (Figure 9a) reveal the presence of Mg, Ca, and Zn elements. The weight percent of Mg is 97.83 %, Zn is 1.93 % and Ca is 0.24 %. This ratio differs from that of the original ratio where Mg is 96.2 %, Zn is 3 % and Ca is 0.8 %. Ratio of elements differs slightly from the parent alloy due to the fact that EDX is a surface analysis technique that performed on a very small area. Keeping in mind that surface composition may differ than the bulk material and also the composition of the analyzed micro area may slightly differ than other areas. Mg alloy after treatment with hydrofluoric acid (Figure 9b) leading to the formation of MgF_2 layer upon the surface of the substrate [26-27] according to the following equation:

$$Mg + 2\ HF \longrightarrow MgF_2 + H_2 \qquad (5)$$

The presence of fluoride ion results from MgF_2 layer. This layer helps in preventing the base material from direct contact between Mg alloy and the atmosphere yielding an oxide layer on the outer surface layer. Introducing magnesium fluoride is beneficial as fluoride is a main constituent of human body. Moreover, it plays a vital role between the coating layer and the metal substrate keeping a chance for enhancing the adhesion between the formed ETELAC/HAP composite coatings. It can be suggested that interlayer helps in EPD process through the formation of MgF_2 that regarded as insulating layer preventing the dissolution of the substrate at the working pH (6.6-7.6) which may cause Mg dissolution. This layer helps in raising the applied potential during EPD.

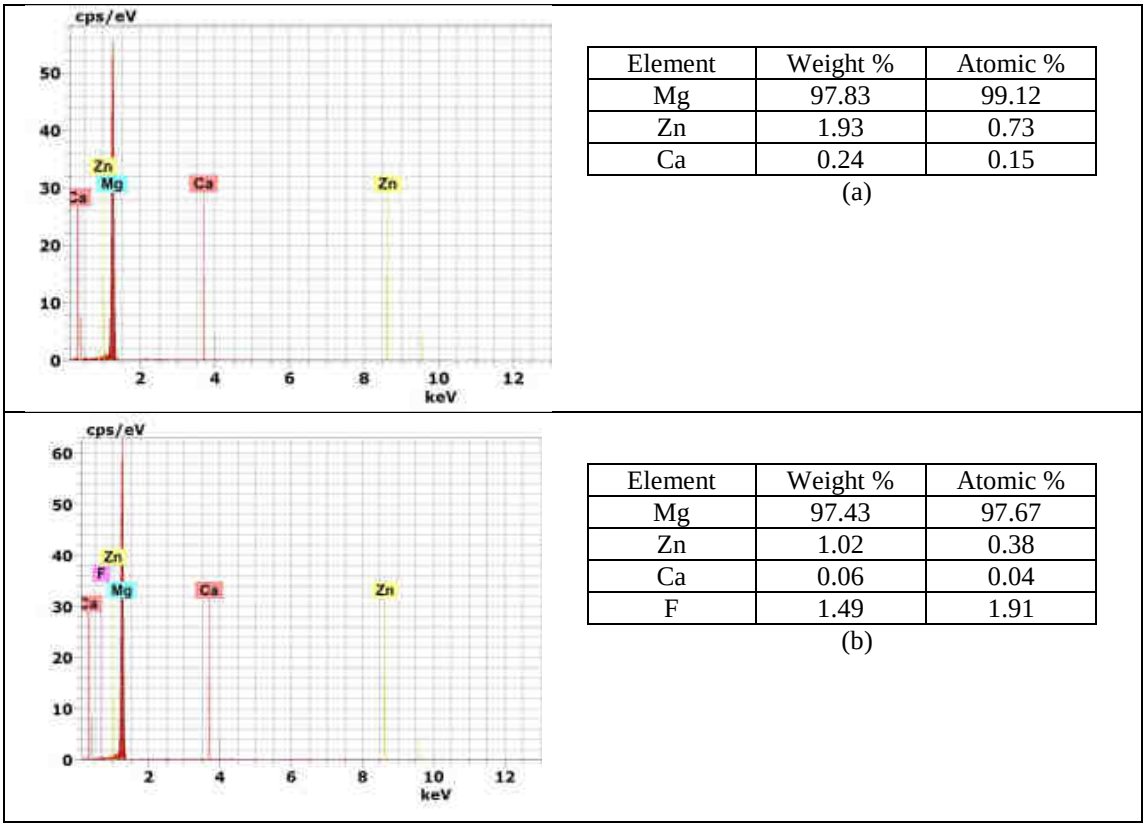

Element	Weight %	Atomic %
Mg	97.83	99.12
Zn	1.93	0.73
Ca	0.24	0.15

(a)

Element	Weight %	Atomic %
Mg	97.43	97.67
Zn	1.02	0.38
Ca	0.06	0.04
F	1.49	1.91

(b)

Figure 9: EDX analysis of (a) Mg alloy and (b) Mg alloy after treatment in HF acid MgF_2 may be formed rapidly on α-Mg phase i.e. on grain matrix rather than grain boundary.

According to XRD curve of Mg alloy, $Ca_2Mg_6Zn_6$ arises on grain boundary that acts as cathode, while α-Mg form grain matrix which undergoes anodic dissolution during pretreatment in HF acid forming a rough surface from MgF_2 layer which may be beneficial in increasing the adhesion of the composite coating [28].

AC-EPD coating samples using 5%ETELAC+5%HAP suspension give granules irregular and not fully smooth in shape (Figure 10) which may be due to the fact that; applying an AC-voltage causes movement of all particles in the bulk of the solution causing deposition of all particle size on the electrode surface yielding a compact coating layer. EDX analysis (Figure11) shows Ca/P ratio doesn't exactly 1.67 as mentioned above, also the elements constituting the ETELAC have higher percent ratio than Ca and P elements forming HAP particles as explained above. Surface characterization analysis shows crack free coating layer of HAP/ETELAC composite coating of finer granules and approximately without any pores.

AC-EPD coating samples using 2.5%ETELAC+5%HAP suspension has low content of Ca and P (Figure 13) as compared to that obtained using 5%ETELAC+5%HAP suspension. Low ETELAC content decreases the dragging of HAP particles to the electrode surface leading to low weight gain. Surface analysis indicates that sponge-like HAP/ETELAC composite coating. The coating layer arranged in different planes. There are many pores in the coating layer although these pores don't penetrate to the substrate (Figure 12) as EDX analysis doesn't give any peaks related to Mg element.

SEM images of AC-EPD coated samples using 2.5%ETELAC+2.5%HAP suspension (Figure 14) reveal the presence of compact, smooth structure with a good coverage of the surface mainly due to the presence of high ETELAC content. It has the lowest content of Ca and P elements constituting HAP particles (Figure 15) . The high content C indicating that the coating layer is almost constituted of ETELAC particles rather than HAP particles due to organic nature of ETELAC. It obvious that composite coatings formed by AC-EPD in all suspension have C percent ratio arranged in this sequence:

2.5%ETELAC+2.5%HAP > 2.5%ETELAC+5%HAP > 5%ETELAC+5%HAP,

Ca and P contents are in contrary to that of C content and have the sequence:

5%ETELAC+5%HAP > 2.5%ETELAC+5%HAP > 2.5%ETELAC+2.5%HAP

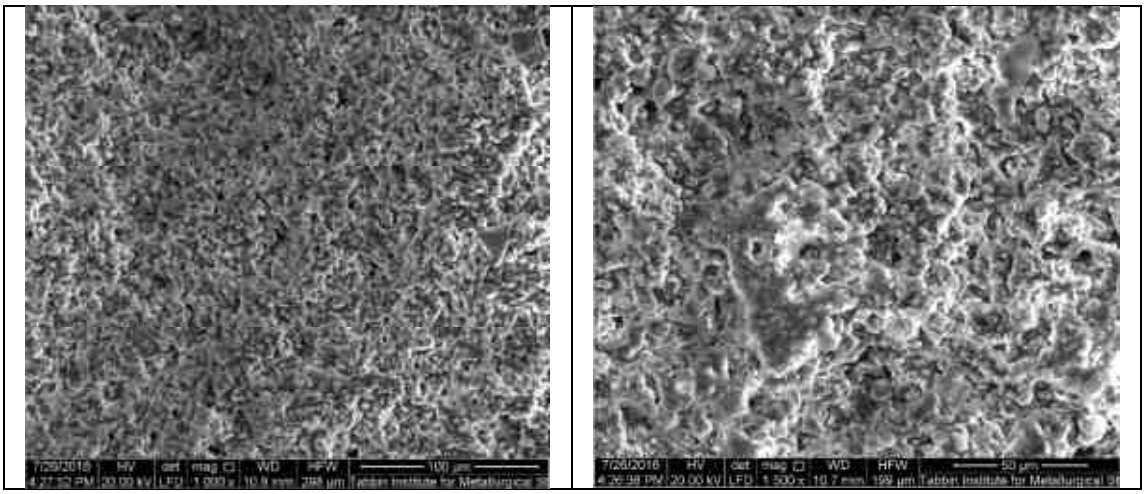

Figure 10: SEM images of AC-EPD coated sample using 5%ETELAC + 5%HAP suspension at 200 V with stirring at 150 r.p.m

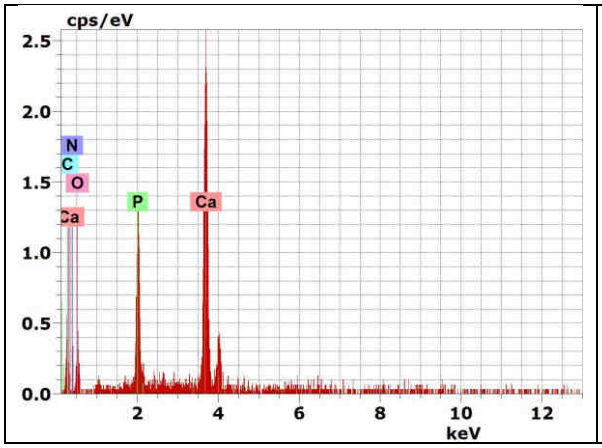

Element	Weight %	Atomic %
O	23.73	27.26
C	29.19	44.68
Ca	30.01	13.77
P	11.28	6.69
N	5.78	7.59

Figure 11: EDX spectra of AC-EPD coated sample using 5%ETELAC + 5%HAP suspension at 200 V with stirring at 150 r.p.m

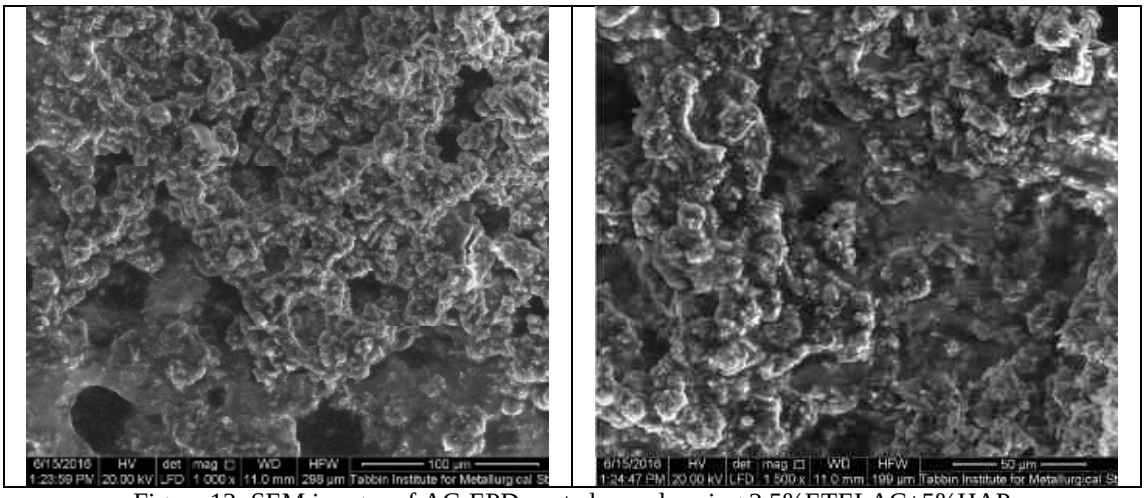

Figure 12: SEM images of AC-EPD coated sample using 2.5%ETELAC+5%HAP suspension at 200 V with stirring at 150 r.p.m

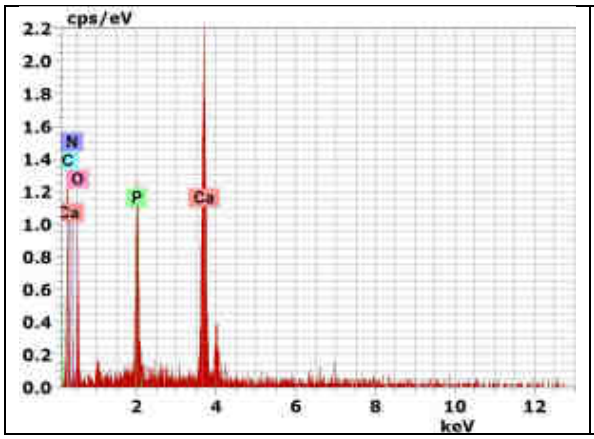

Element	Weight %	Atomic %
O	31.40	32.26
C	36.96	50.58
Ca	14.17	7.68
P	8.32	4.41
N	4.16	4.88

Figure 13: EDX spectra of AC-EPD coated sample using 2.5%ETELAC + 5%HAP suspension at 200 V with stirring at 150 r.p.m

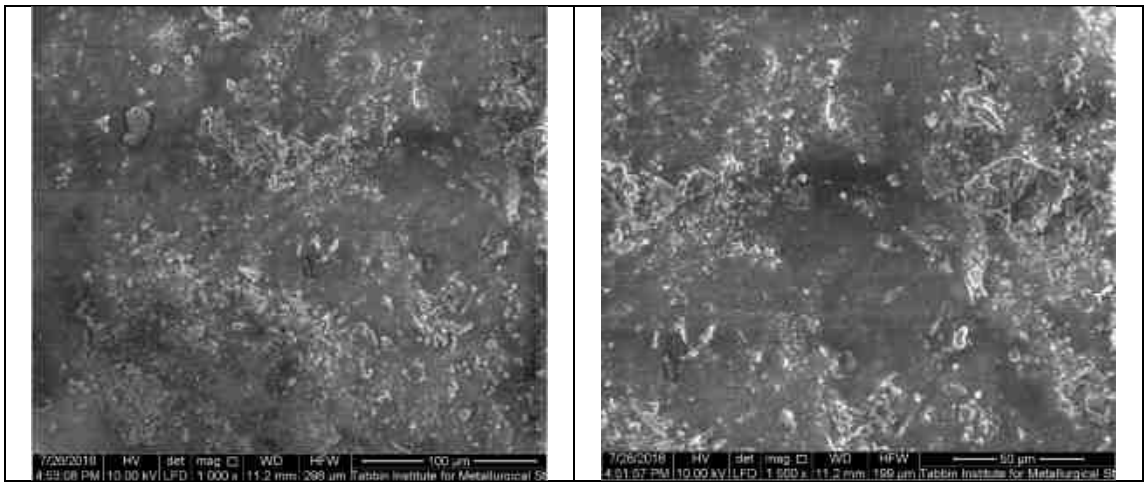

Figure 14: SEM images of AC-EPD coated sample using 2.5%ETELAC+2.5%HAP suspension at 200 V with stirring at 150 r.p.m

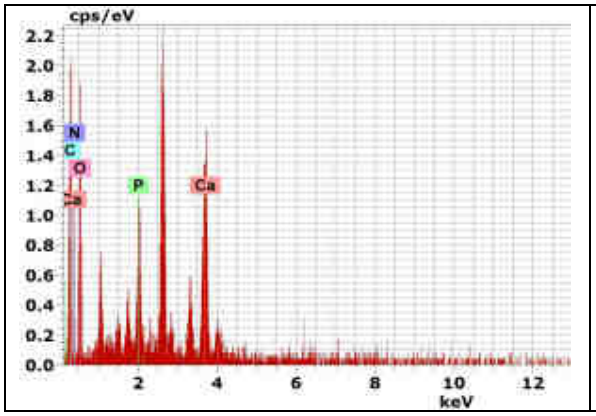

Element	Weight %	Atomic %
O	41.32	40.64
C	38.89	49.76
Ca	11.99	4.60
P	4.08	2.02
N	2.72	2.98

Figure 15: EDX spectra of AC-EPD coated sample using 2.5%ETELAC+2.5%HAP suspension at 200 V with stirring at 150 r.p.m

3.4.3. Adhesion Test (Adhesion tape test)

Adhesion test carried out according to ASTM D3359 standard test methods for measuring adhesion by Tape Test [29] and results are shown in Table (6) and Figure 16.

Table (6): Rating of adhesion test

No.	Applied voltage	Suspension concentration	Rating
1	DC-EPD	5%ETELAC + 5%HAP	5A
2	DC-EPD	Ultrasonic 5%ETELAC + 5%HAP	5A
3	AC-EPD	5%ETELAC + 5%HAP	5A
4	DC-EPD	2.5%ETELAC + 5%HAP	5A
5	AC-EPD	2.5%ETELAC + 5%HAP	5A
6	DC-EPD	2.5%ETELAC + 2.5%HAP	5A
7	AC-EPD	2.5%ETELAC + 2.5%HAP	5A

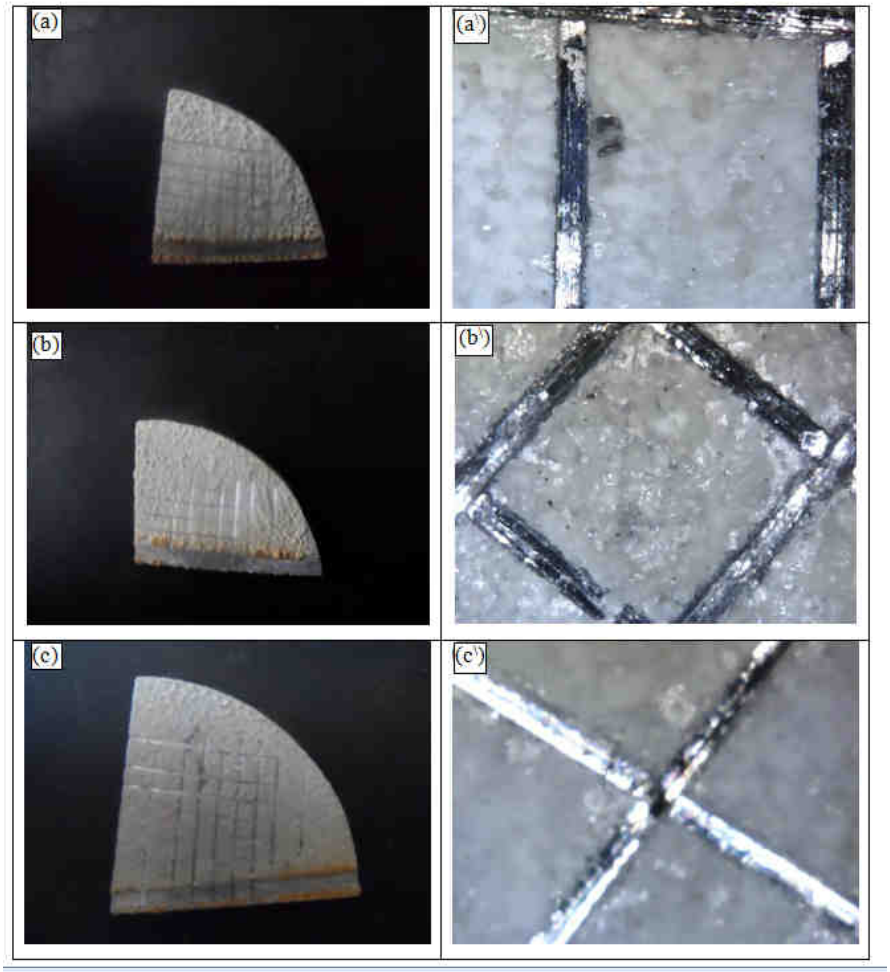

Figure 16: AC-EPD coated sample using: (a) 5%ETELAC + 5%HAP suspension at 220 V with stirring at 150 r.p.m; (b) 2.5%ETELAC + 5%HAP suspension at 200 V with stirring at 150 r.p.m; (c) 2.5%ETELAC + 5%HAP suspension at 200 V with stirring at 150 r.p.m. Note that a,b,c images were taken by digital camera while a', b',c ' were taken by optical microscope

All deposited coating layers adhere well with the magnesium alloy substrate without peeling off. It can be concluded that ETELAC and hydroxyapatite (HAP) can produce ceramic coating with high interfacial bond strength.

3.4.4. Electrochemical measurements

EIS measurements of magnesium alloy before and after treatment in 40% HF and after coating with ETELAC/HAP composite coating samples were carried out in Hank's solution at open circuit potential (OCP). The results are presented in Figures 17-18 and Table (7). In the Nyquist plot the real part of the impedance is plotted on the X-axis and the imaginary part is plotted on Y-axis. EIS results show a one capacitance loop along all frequency regions. Bode plots refer to the presentation of the impedance magnitude (the average value between the real and imaginary values) relative to frequency. Because both the impedance and frequency often span orders of magnitude, they are frequently plotted on a logarithm scale. Bode plots explicitly show the frequency-dependence of the impedance of the device under test. Nyquist plots indicate that activation-

controlled processes with distinct time-constants show up as unique impedance arcs and the shape of the curve provides insight into possible mechanism or governing phenomena. However, this format of representing impedance data has the disadvantage that the frequency-dependence is implicit; therefore, the AC frequency of selected data points should be indicated. Because both data formats have their advantages, it is usually best to present both Bode and Nyquist plots. Figure 18 shows the Nyquist and Bode plots of magnesium alloy before and after treatment in 40% HF at OCP.

Mg alloy before and after treatment in 40% HF give almost the same result with a slight increase in $Z^{\backslash}$ value for the alloy after HF treatment (5812 Ω cm^2 & 5617 (Ω cm^2). The negative value is observed in the imaginary part at low frequencies indicating inductive properties of formed MgF_2 layer. The same tendency is observed for Bode plot. At low frequencies, slight increase in the log $|Z|$ value in case of HF treated alloy compared to the untreated alloy which may be attributed to the formation of MgF_2 layer resulting in more corrosion resistance.

EIS spectra of coated samples (Figure 18) show more corrosion resistance than uncoated Mg alloy. Coated samples using 5%ETELAC + 5%HAP suspension gives impedance amounts to 107.900(KΩ cm^2), the coated samples using 2.5%ETELAC + 5%HAP suspension gives 289.700 (KΩ cm^2), while the coated samples using 2.5%ETELAC + 2.5%HAP suspension gives 1484.000 (KΩ cm^2). Bode plots indicated that at low frequencies region, coated samples using 5%ETELAC + 5%HAP suspension record $|Z|$ value equals 104.472 KΩ, the corresponding value for coated samples using 2.5%ETELAC + 5%HAP suspension equals 262.421 KΩ, while the coated samples using 2.5%ETELAC + 2.5%HAP suspension records 1489.361 KΩ. In case of AC experiment, the relatively low concentration of the ETELAC polymer facilitate the response of HAP particles towards electric field in all directions resulting in a more compact coating. Corrosion resistance for coated samples using AC-EPD shows the following sequence:

2.5%ETELAC + 2.5%HAP > 2.5%ETELAC + 5%HAP > 5%ETELAC + 5%HAP

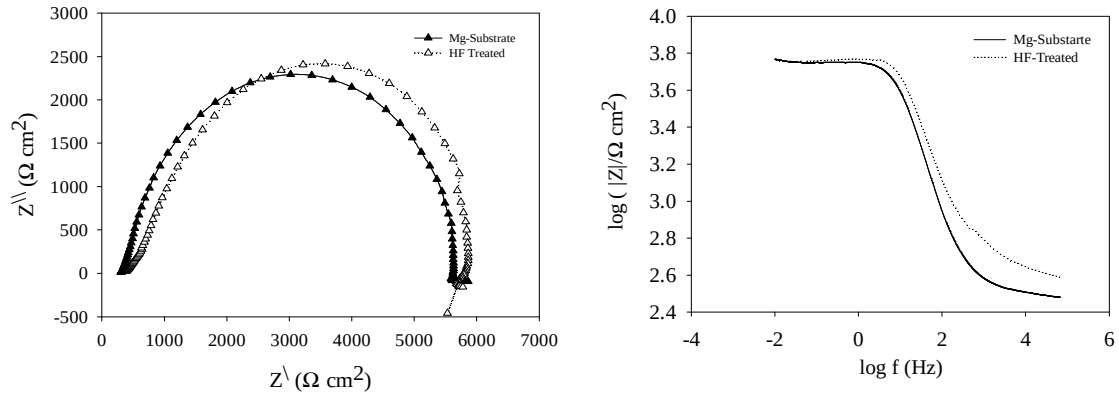

Figure 17: Nyquist and Bode plot for Mg alloy and Mg alloy after treatment in 40% HF

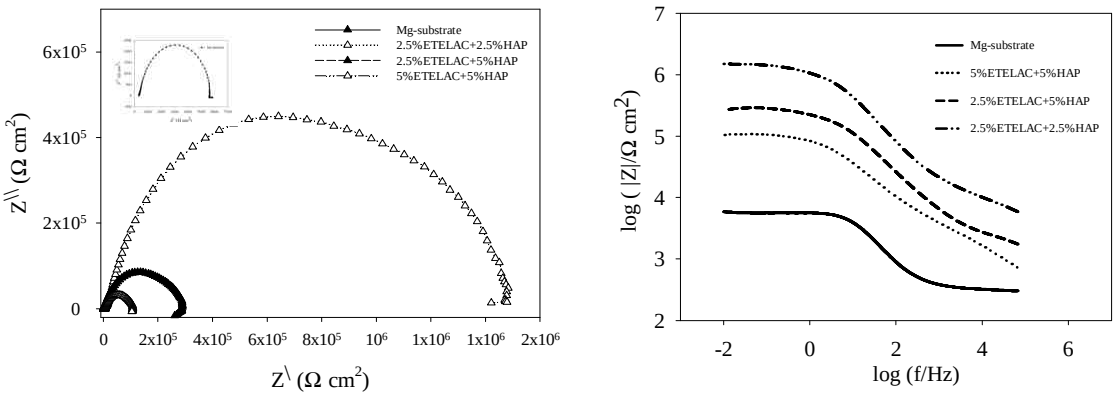

Figure 18: Nyquist and Bode plot for Mg alloy and Mg coated samples obtained using AC-EPD

In general, it can be stated that, corrosion resistance increases with the increase of the capacitive loop or increase in the diameter of the obtained semicircle in case of Nyquist plots and increase with the increase of log $|Z|$ value at low frequency in case of Bode plots.

Table (7): Impedance data of coated samples

Samples	R_S (Ω)	R_P (Ω)	C_{dl} (µF)
Mg-substrate	418.431	5229.80	4.0712
HF-treated	397.720	5315.42	2.53456
DC-5%ETELAC+5%HAP	496.889	5268.37	1.72683
AC-5%ETELAC+5%HAP	464.435	102440	1.13445
U.S-5%ETELAC+5%HAP	1081.76	1142180	0.857844
DC-2.5%ETELAC+5%HAP	1953.27	36787.2	0.928175
AC-2.5%ETELAC+5%HAP	1322.57	284214	0.412169
DC-2.5%ETELAC+2.5%HAP	2789.73	403105	0.242162
AC-2.5%ETELAC+2.5%HAP	6387.17	1479140	0.112174

4. Conclusions

AC-EPD is a promising method to achieve high performance HAP/ETELAC composite coating. Introducing an alternative field causes the oscillation of the deposited particles leading their rearrangement into a more favorable packing structure. The highest performance ETELAC/HAP composite coatings was obtained using 5% ETELAC+ 5% HAP suspension under conditions of 200 V, 150 rpm stirring and multi-run (M) deposition. The ETELAC/HAP composite coatings corrosion resistance was largely improved in comparison to the base Mg alloy.

5. References

1. M. Navarro, A. Michiardi, O Castaño, JA Planell, Journal of The Royal Society Interface, 2008. 5(27): p. 1137-1158.
2. R. Van Noort, Journal of Material Science, Vol.22, (1987), pp. 3801-3811.
3. M. Savioli Lopes, A. L. Jardini, R. Maciel Filho, Procedia Engineering 42 (2012) 1402-1413.
4. Sivakumer M. and Manjubala I., Mater. Lett. 50 (2001) 199.
5. Kumer R. and Wang M., Mater. Lett. 55(2002) 133.
6. Wang J., Chao Y., Wanb Q., Zhu Z. and Yu H., Acta Biomaterialia, 5 (2009) 1798.
7. Alejandra Chávez-Valdez, Aldo R. Boccaccini, Electrochimica Acta 65 (2012) 70-89.
8. G.L. Song, Corros Sci, 49 (2007) 1696.
9. B. Viswanath, V.V. Shastry, U. Ramamurty, N. Ravishankar, Acta Mater. 58 (2010) 4841-4848.
10. K Suchanek, A Bartkowiak, A Gdowik, M Perzanowski, S Kąc, B Szaraniec, M Suchanek, M Marszałek, Mater Sci Eng C 51 (2015) 57-63
11. J. Liu, K. Li, H. Wang, M. Zhu, H. Xu, H. Yan, Nanotechnology 16 (2005) 82.
12. H. Tamai, H. Yasuda, Journal of Colloid and Interface Science 212, 585-588 (1999).
13. D.M. Ibrahim, W.H. Hegazy, A.E. Mahgoub and H. Abo-Elmajed, Common. Fac. Sci. Univ. Ank Series B. V. 46. PP 33-46 (200).
14. Kappe CO, Angew Chem Int. Edn, 43, 2004, 6256.
15. I. Zhitomirsky, Advances in Colloid and Interface Science 97 (2002) 277-315.
16. X.F. Xiao, R.F. Liu, , Materials Letters 60 (2006) 2627-2632.
17. Chavez-Valdez A, Boccaccini AR. Electrochimica Acta. 2012; 65: 70.
18. Zhitomirsky I, Gal-or L., J Mater Sci: Mater Med 1997; 8: 213-9.
19. M. Javidi, S. Javadpour, M.E. Bahrololoom, J. Ma, Mater Sci Eng C 28 (2008) 1509-1515.
20. Cho J, Konopka K, Rozniatowski K, Garcia-Lecina E, Shaffer MSP, Boccaccini AR. Carbon. 2009; 47: 58
21. T. Yui, Y. Mori, T. Tsuchino, T. Itoh, T. Hattori, Y. Fukushima, K. Takagi, Chem. Mater. 17 (1) (2005) 206-211.
22. M.J. Santillán, F. Membrives, N. Quaranta, A.R. Boccaccini, J. Nanoparticle Res. 10 (5) (2008) 787-793.
23. S. Radice, M. Stefano, M. Johann, Key Eng Mater. 412 (2009) 51-56.
24. S. Radice, C.R. Bradbury, J. Michler, S. Mischler, J. Eur. Ceram. Soc. 30 (5) (2010) 1079-1088.
25. H. R. Bakhsheshi-Rad, E. Hamzah, A. Fereidouni-Lotfabadi, M. Daroonparvar, M. A. M. Yajid, M. Mezbahul-Islam, M. Kasiri-Asgarani and M. Medraj, Materials and Corrosion 2014, DOI: 10.1002/maco.201307588.
26. A.W. Goldenstein, W. Rostoker, F. Schossberger, J. Electrochem. Soc. 104 (1957) 104.
27. Y. Xiang, W. Hu, X. Liu, C. Zhao, W. Ding, Trans. Inst. Met. Finish. 79 (2001) 30.
28. Ibrahim M. Ghayad, Hassan H. Elsentriecy, Zeinab A. Abdel Aziz, EuroCorr 2013, 1-5 Sept. 2013, Portugal.
29. Lakshmi RV, Basu BJ. Journal of Colloid and Interface Science. 2009; 339: 454.